# X-ray Crystallographic Studies of Alanine-65 Variants of Carbonic Anhydrase II Reveal the Structural Basis of Compromised Proton Transfer in Catalysis†

Laura R. Scolnick and David W. Christianson*

*Department of Chemistry, University of Pennsylvania, Philadelphia, Pennsylvania 19104-6323*

*Received July 19, 1996; Revised Manuscript Received September 18, 1996*⊗

ABSTRACT: The three-dimensional structures of A65F, A65L, A65H, A65T, A65S, and A65G human carbonic anhydrase II (CAII) variants have been solved by X-ray crystallographic methods to probe the importance of residue 65 and the structural implications of its evolutionary drift in the greater family of carbonic anhydrase isozymes. Structure−activity relationships in this series of CAII variants are correlated with those established for other carbonic anhydrase isozymes. We conclude that a bulky side chain at position 65 hinders the formation of an effective solvent bridge between zinc-bound water and H64 and thereby hinders solvent-mediated proton transfer between these two groups [Jackman, J. E., Merz, K. M., Jr., & Fierke, C. A. (1996) *Biochemistry 35*, 16421−16428]. Despite the introduction of a polar hydroxyl group at this position, smaller side chains such as serine or threonine substituted for A65 do not perturb the formation of a solvent bridge between H64 and zinc-bound solvent. Thus, the evolution of residue 65 size is one factor affecting the trajectory of catalytic proton transfer.

The carbonic anhydrase (CA)[1] family of zinc metalloenzymes consists of seven known isozymes which catalyze the hydration of carbon dioxide to yield bicarbonate ion and a proton. This reaction occurs via two distinct chemical steps (Silverman & Lindskog, 1988; Lindskog & Liljas, 1993; Christianson & Fierke, 1996): (1) nucleophilic attack of zinc-bound hydroxide at substrate $CO_2$ and (2) following the exchange of product bicarbonate with a water molecule, the regeneration of zinc-bound hydroxide from zinc-bound water by the transfer of a proton to bulk solvent. The rate constant $k_{cat}$ generally reflects proton transfer between zinc-bound water and an active site "shuttle" residue in the second step; subtle structural differences among the CA isozymes contribute to the wide range of $k_{cat}$ values ($10^3$−$10^6$ $s^{-1}$) measured for this step in different isozymes. Indeed, different residues may function as an intermediary proton shuttle between zinc-bound water and bulk solvent in different isozymes. For instance, H64 is the catalytic proton shuttle in CAII ($k_{cat} = 1 \times 10^6$ $s^{-1}$) (Steiner et al., 1975; Tu et al., 1989), and it is hydrogen bonded to zinc-bound water through bridging solvent molecules across which the product proton must be transferred (Håkansson et al., 1992). The side chain of H200 is the best candidate for a proton shuttle in CAI ($k_{cat} = 2 \times 10^5$ $s^{-1}$) (Khalifah, 1971) due to its proximity to the zinc ion and its p$K_a$ (Engstrand et al., 1995). In contrast, there appears to be no proton shuttle in the active site of CAIII ($k_{cat} = 1 \times 10^4$ $s^{-1}$), where the product proton is probably transferred directly to bulk solvent (Jewell et al., 1991).

The structure of murine mitochondrial isozyme V (CAV) has been determined and refined at 2.0 Å resolution (Boriack-Sjodin et al., 1995, 1996). Like isozyme II, CAV is roughly spherical, and the active site lies within a conical cleft about 15 Å deep. Although the zinc binding sites and substrate binding pockets of CAII and CAV are virtually identical, active site structures diverge significantly in the region of residue 64: CAII has H64, whereas CAV has Y64. Moreover, Y64 does not appear to function as the major proton shuttle group (Heck et al., 1994), and the environment of residue 64 may contribute to this behavior. In CAII, the sequence G63-H64-A65 is found, but in CAV the corresponding sequence is G63-Y64-F65. Comparison of the CAII and CAV structures suggests that F65 of CAV alters the steric contour of the active site sufficiently enough to block, or at least hinder, effective proton transfer between zinc-bound water and residue 64 across a bridging solvent network (Boriack-Sjodin et al., 1995). Indeed, effective proton transfer to histidine in the Y64H variant of CAV is achieved only when accompanied by a second amino acid substitution, F65A, which alleviates the steric blockage (Heck et al., 1996).

Sequence analysis of residues 63−65 among different CA isozymes reveals interesting patterns of divergence. Residue G63 is shown to be highly conserved throughout the CA family except for rat CAIV which has Q63. Inspection of the human CAII structure shows that this glycine is required to maintain a specific turn conformation. A non-glycine residue at this position would not maintain this turn conformation since it would have to adopt backbone $\phi$, $\psi$ angles falling in a disallowed region of the Ramanchandran plot. In contrast, residues 64 and 65 of the CA active site have significantly diverged among different CA isozymes from different sources (Table 1), despite the conservation of other active site features (e.g., the hydrophobic substrate binding pocket and the zinc binding site) among this same group of proteins (data not shown). Thus, although the CA isozymes retain similar active site structures to achieve the

† Supported by NIH Grant GM45614 and Cell and Molecular Biology Training Grant GM07229.

* Author to whom correspondence should be addressed: (215) 898-5714 (phone); (215) 573-2201 (fax); chris@xtal.chem.upenn.edu (email).

⊗ Abstract published in *Advance ACS Abstracts,* December 1, 1996.

[1] Abbreviations: CA, carbonic anhydrase; CAI, carbonic anhydrase I; CAII, carbonic anhydrase II; CAIII, carbonic anhydrase III; CAIV, carbonic anhydrase IV; CAV, carbonic anhydrase V; CAVI, carbonic anhydrase VI; CAVII, carbonic anhydrase VII.

S0006-2960(96)01787-4 CCC: $12.00 

Table 1: Carbonic Anhydrase Residue 63−65 Sequence Comparison[a]

| | | | |
|---|---|---|---|
| CAI | | CAIII | |
| human | GHS | human | GKT |
| chimp | GHS | mouse | GRT |
| rhesus | GHS | rat | GKT |
| ox | GHS | ox | GKT |
| horse | GHS | gorilla | GKT |
| orang | GHS | horse | GRT |
| rabbit | GHS | | |
| turtle | GHS | CAIV | |
| mouse | GHS | human | GHS |
| pig tail | GHS | rat | QHS |
| CAII | | CAV | |
| human | GHA | human | GYL |
| mouse | GHS | mouse | GYF |
| bovine | GHS | | |
| rat | GHS | CAVI | |
| rabbit | GHS | human | GHT |
| ox | GHS | sheep | GHT |
| sheep | GHS | | |
| horse | GHS | CAVII | |
| rhesus | GHS | human | GHS |
| chicken | GHS | | |

[a] Sequence data abstracted from Fleming et al. (1993) and Hewett-Emmett et al. (1984) and references cited therein.

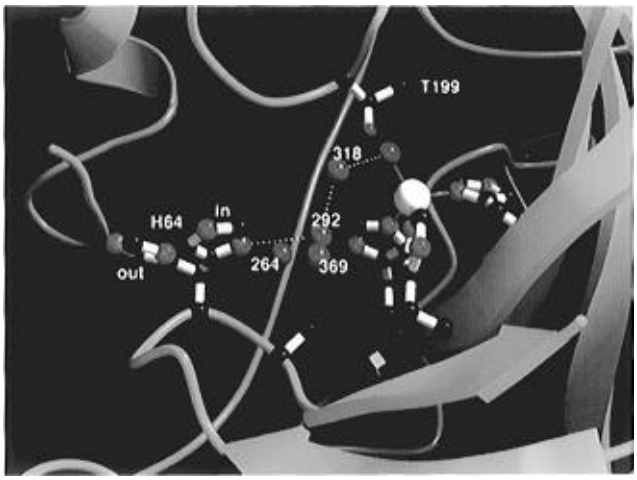


FIGURE 1: Active site of human carbonic anhydrase II, showing important active site solvent molecules as observed in the 1.54 Å resolution structure of the native enzyme (red spheres) (Håkansson et al., 1992). Zinc appears as a white sphere. Proton transfer in catalysis occurs across a solvent bridge between the zinc-bound solvent and the side chain of H64. The out conformation of H64 is also indicated to illustrate the conformational mobility of this residue (Krebs et al., 1991; Nair & Christianson, 1991). The short side chain of A65 allows for the optimal assembly of this solvent bridge. Figure generated with Molscript (Kraulis, 1991) and Raster3D (Bacon & Anderson, 1988; Meritt & Murphy, 1994).

first step of catalysis, they have clearly diverged in terms of the structural and chemical requirements of the second step of catalysis, proton transfer from zinc-bound water to bulk solvent. In CAII, the proton acceptor is H64 (Tu et al., 1989; Krebs et al., 1991), and its side chain is observed in two possible conformations with respect to the active site zinc ion (Figure 1): "in" (directed toward zinc) (Håkansson et al., 1992) and "out" (directed away from zinc) (Alexander et al., 1991; Nair & Christianson, 1991). Due to its proximity, residue 65 may play an important role in modulating the conformation and the possible proton shuttling properties of residue 64.

In order to probe structure−function relationships for residue 65 and the implications of its evolutionary drift in the family of CA isozymes, we have prepared and analyzed A65 variants of CAII. In this work, we report the three-dimensional structures of the A65F, A65L, A65H, A65T, A65S, and A65G variants, and we correlate these structures with activity measurements made by Jackman et al. (1996). This work conclusively demonstrates that a bulky side chain at position 65 of CAII sterically hinders the formation of a catalytically optimal solvent bridge between zinc-bound water and H64. For reference, the CAII active site is shown in Figure 1.

## MATERIALS AND METHODS

Recombinant CAII variants were generously provided by Professor Carol Fierke and were crystallized by the sitting drop method. Typically, a 7 $\mu$L drop containing enzyme and 50 mM Tris-HCl (pH 8.0 at room temperature) was added to a 7 $\mu$L drop containing 50 mM Tris-HCl (pH 8.0 at room temperature) and 1.95−3.9 M ammonium sulfate in the crystallization well; this drop was equilibrated against 1 mL of precipitant buffer in the well reservoir. Protein solutions of A65H, A65L, and A65T CAIIs were saturated with methylmercury acetate in order to facilitate the growth of diffraction-quality parallelpipedons. Dithiothreitol (2 mM) was added to the protein solution of A65F and A65S in order to facilitate the growth of plate-like crystals suitable for data collection. Thin plates of A65G were grown in the presence of saturated methylmercury acetate and 2 mM dithiothreitol. All CAII variants crystallized isomorphously with the wild-type enzyme (Alexander et al., 1991) and belonged to space group $P2_1$ with typical unit cell parameters of $a = 42.7$ Å, $b = 41.7$ Å, $c = 73.0$ Å, and $\beta = 104.6°$. In addition, A65S CAII also crystallized in orthorhombic space group $P2_12_12_1$ with unit cell parameters $a = 42.5$ Å, $b = 72.5$ Å, $c = 75.1$ Å, and $\alpha = \beta = \gamma = 90°$. This alternate space group has been observed only twice before, when amino acid substitutions in the metal binding site resulted in partial zinc occupancy (Alexander et al., 1991; Ippolito, 1995).

Crystals of each variant were mounted in 0.5 or 0.7 mm glass capillaries with a small portion of mother liquor and sealed with wax. X-ray diffraction data were collected using an R-AXIS IIc image plate detector mounted on an RU-200HB rotating anode generator with double focusing mirrors operating at 50 kV/100 mA. Data were collected in successive 12−15 min 2° or 3° oscillations about $\phi$ for a total scan of 120°; the crystal-to-detector distance was set at 90 or 105 mm, and the swing angle $2\theta$ was set at 0°. The crystal orientation was established with REFIX (Kabsch, 1993), and data were reduced using MOSFLM (Leslie, 1992). Data reduction was completed with CCP4 (Collaborative Computational Project 4, 1994); relevant statistics are recorded in Table 2.

The starting coordinate set for the refinement of each monoclinic variant was that of native CAII (Håkansson et al., 1992) with the A65 side chain and all water molecules deleted from the model. The structure of each CAII variant was refined by simulated annealing with energy minimization as implemented in X-PLOR (Brünger et al., 1987). When the crystallographic *R*-factor dropped below 0.20 in each refinement, the variant side chain and waters were modeled into electron density maps generated with Fourier coefficients $2|F_o| - |F_c|$ and $|F_o| - |F_c|$ and phases calculated from the in-progress atomic model. In A65H CAII, coordinates for two partially occupied conformers of H65 were built into

Table 2: Data Collection and Refinement Statistics for A65 CAII Variants

| | A65F | A65H | A65L | A65T | A65S | A65S[d] | A65G |
|---|---|---|---|---|---|---|---|
| no. of crystals | 1 | 1 | 1 | 1 | 1 | 1 | 1 |
| no. of measured reflections | 20445 | 51671 | 44276 | 41320 | 40095 | 27183 | 39629 |
| no. of unique reflections | 10085 | 15547 | 18353 | 17315 | 16488 | 11298 | 16603 |
| maximum resolution (Å) | 2.3 | 2.0 | 1.9 | 2.0 | 2.0 | 2.2 | 2.0 |
| completeness of data (%) | 88.1 | 92.5 | 87.1 | 94.7 | 96.7 | 92.7 | 96.7 |
| $R_{sym}$[a] | 10.3 | 4.8 | 4.3 | 5.9 | 8.4 | 9.1 | 9.2 |
| no. of water molecules in final cycle of refinement | 117 | 110 | 117 | 106 | 119 | 61 | 121 |
| no. of reflections used in refinement ($>2\sigma$) | 9422 | 15077 | 17507 | 15881 | 16765 | 10574 | 16046 |
| $R_{cryst}$[b] | 0.154 | 0.162 | 0.714 | 0.173 | 0.176 | 0.179 | 0.175 |
| $R_{free}$[c] | 0.246 | 0.225 | 0.229 | 0.232 | 0.255 | 0.282 | 0.235 |
| rmsd, bonds (Å) | 0.009 | 0.008 | 0.006 | 0.007 | 0.009 | 0.010 | 0.009 |
| rmsd, angles (deg) | 1.6 | 1.5 | 1.6 | 1.5 | 1.6 | 1.8 | 1.6 |
| rmsd, dihedrals (deg) | 25.3 | 25.5 | 25.4 | 25.2 | 25.5 | 25.9 | 25.2 |
| rmsd, impropers (deg) | 1.4 | 1.2 | 1.3 | 1.4 | 1.5 | 1.6 | 1.3 |

[a] $R_{sym} = \Sigma|I_i - \langle I_i\rangle|/\Sigma\langle I_i\rangle$; $I_i$ = intensity measured for reflection $i$; $\langle I_i\rangle$ = average intensity for reflection i calculated from replicate data. [b] $R_{cryst} = \Sigma||F_o| - |F_c||/\Sigma|F_o|$; $|F_o|$ and $|F_c|$ are the observed and scaled calculated structure factors, respectively. [c] $R_{free} = \Sigma||F_o| - |F_c||/\Sigma|F_o|$ calculated for reflections belonging to a test set of 10% of the unique reflections omitted from refinement. [d] Orthorhombic crystal form.

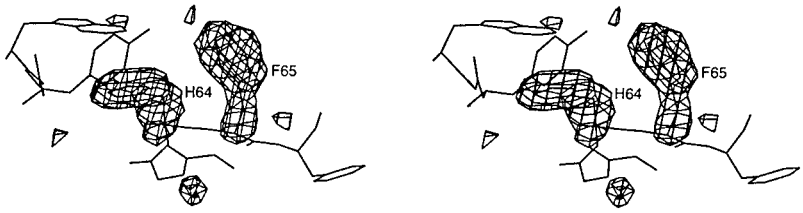


FIGURE 2: Difference electron density map of A65F CAII, generated with Fourier coefficients $|F_o| - |F_c|$ and phases calculated from the final model less the atomic coordinates of F65 and H64. The map is contoured at $2.7\sigma$. Refined atomic coordinates are superimposed; H64 and F65 are indicated. H64 adopts the out conformation.

the electron density map and refined satisfactorily. The graphics software CHAIN (Sack, 1988) installed on a Silicon Graphics Indigo workstation was utilized for all map-fitting procedures. Electron density peaks in the solvent region were interpreted as water molecules if their peak heights were $>2.5\sigma$, if they were found within hydrogen-bonding distance of appropriate protein atoms, and if they refined with thermal *B*-factors $\leq 50$ Å$^2$.

Initial phases for the electron density map of the orthorhombic crystal form of A65S CAII were obtained by molecular replacement using AMoRe (Navaza, 1994) as implemented in CCP4. The atomic coordinates of the refined monoclinic A65S CAII structure were used as a search probe in rotation and translation functions. The highest peak in the cross-rotation function was at $22.7\sigma$ ($\alpha = 62.3°$, $\beta = 60.8°$, $\gamma = 173.2°$); a subsequent translation search yielded a $16.2\sigma$ solution at Tx = 0.3893, Ty = 0.3434, and Tz = 0.2265. Rigid body refinement lowered the crystallographic *R*-factor from 0.34 to 0.30, and the structure was refined to convergence.

For each variant refinement converged smoothly to final crystallographic *R*-factors within the range 0.154−0.179; all pertinent refinement statistics are recorded in Table 2. For each structure, the rms error in atomic positions was estimated to be ca. 0.2−0.3 Å using SIGMA-A (Read, 1986). Atomic coordinates have been deposited in the Brookhaven Protein Data Bank (Bernstein et al., 1977).[2]

## RESULTS AND DISCUSSION

The overall structure of each CAII variant in the monoclinic crystal form is very similar to that of the wild-type enzyme, and the rms deviation of Cα atoms between each variant and the wild-type enzyme is only 0.21−0.28 Å. In all six CAII variants only the backbone atoms of N-terminal residues H3 and H4 have good electron density; therefore, H3 and H4 are included in the final coordinate sets, but the occupancies of side chain atoms are set to zero. In both A65F and A65H there is no electron density for the side chain of C-terminal K261; therefore, main chain atoms of K261 are included in the final coordinate set, but the occupancy of its side chain is set to zero. Zinc−ligand distances in each variant are similar to those observed in the wild-type enzyme. However, active site solvent structure differences are required by the substitution of bulky side chains at position 65.

The difference electron density map of A65F CAII in Figure 2 reveals that F65 protrudes into the active site. The least-squares superposition of A65F with native enzyme (Håkansson et al., 1992) in Figure 3 shows that the bulky side chain of F65 sterically requires the displacement of three active site water molecules observed in the native enzyme (Figure 1): 264, 292, and 369. Water molecule 292 is part of a two-water solvent bridge with water 318 between zinc-bound solvent and H64 in the native enzyme; water molecules 264 and 369 are part of alternate, three-water solvent bridges. Clearly, a bulky side chain at position 65 significantly perturbs solvent structure around H64. Additionally, the bulky F65 side chain causes H64 to rotate away from the active site to the out conformation ($\Delta\chi_1 = 93°$, $\Delta\chi_2 = 20°$).

Similar features are observed in the active site of A65L CAII. The electron density of this variant reveals that the side chain of L65 protrudes into the active site, although to a lesser degree than that observed for the larger F65 side chain in A65F CAII (data not shown). Nevertheless, the least-squares superposition of A65L and wild-type CAIIs in

[2] Accession codes: 1UGA, A65F CAII; 1UGC, A65H CAII; 1UGE, A65L CAII; 1UGF, A65T CAII; 1UGD, A65S CAII (monoclinic); 1UGG, A65S CAII (orthorhombic); 1UGB, A65G CAII.

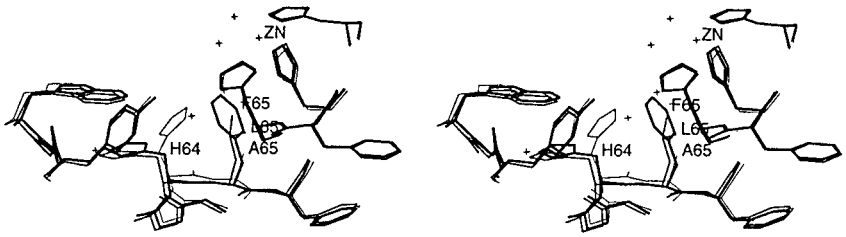


FIGURE 3: Least-squares superposition of A65F (thick bonds), A65L (medium bonds), and native (thin bonds) CAIIs. Residue 65, H64, and zinc are indicated. Solvent molecules from the native structure are represented by unlabeled crosses.

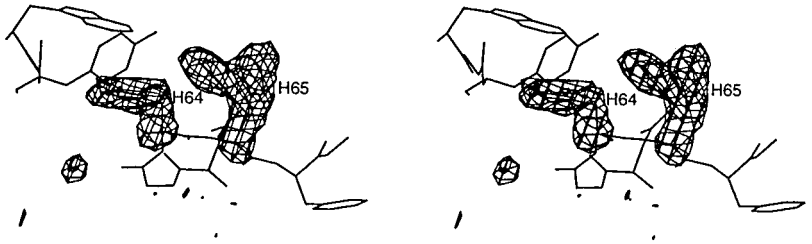


FIGURE 4: Difference electron density map of A65H CAII, generated with Fourier coefficients $|F_o| - |F_c|$ and phases calculated from the final model less the atomic coordinates of H65 and H64. The map is contoured at 2.5$\sigma$. Refined atomic coordinates are superimposed; H64 and H65 are indicated. Note that the electron density for H65 is consistent with two mutually exclusive conformations. H64 adopts the out conformation.

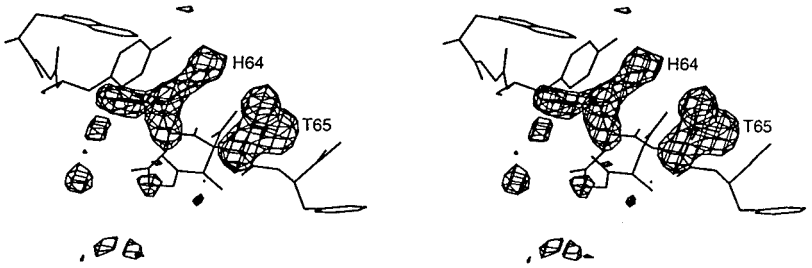


FIGURE 5: Difference electron density map of A65T CAII, generated with Fourier coefficients $|F_o| - |F_c|$ and phases calculated from the final model less the atomic coordinates of T65 and H64. The map is contoured at 2.4$\sigma$. Refined atomic coordinates are superimposed; H64 and T65 are indicated. Note that the electron density for H64 is consistent with a mixed population of in and out conformers.

Figure 3 shows that, like F65, the side chain of L65 is sufficiently bulky to cause the displacement of active site water molecules 264, 292, and 369, as well as the rotation of H64 to the out conformation ($\Delta\chi_1 = 102°$, $\Delta\chi_2 = 20°$).

The observed conformation of the H65 side chain in A65H CAII contrasts with that of phenylalanine or leucine side chains substituted at this position, in that H65 protrudes into the active site and adopts two partially occupied conformations (Figure 4). These conformers are related by a 79° difference in side chain torsion angle $\chi_1$ and a 6° difference in side chain torsion angle $\chi_2$, and they refine with approximate occupancies of 40% and 60%. Each of the histidine conformers is within hydrogen-bonding distance of surrounding residues. The N$\epsilon$ of one conformer may accept hydrogen bonds from the side chain amide groups of N62 and N67. The N$\epsilon$ of the second conformer may hydrogen bond with the hydroxyl group of Y7, while the N$\delta$ of the second conformer may accept a hydrogen bond from the side chain amide group of N244 or donate a hydrogen bond to the backbone carbonyl of F95. As found in A65F and A65L CAIIs, both conformers of H65 sterically require the displacement of water molecules 264, 292, and 369. Additionally, the bulky H65 side chain causes H64 to rotate away from the active site to the out conformation ($\Delta\chi_1 = 103°$, $\Delta\chi_2 = 20°$). It is clear that bulky amino acid substitutions at position 65 will force the adjacent side chain of H64 into the out conformation, but it should be noted that this conformational change alone does not compromise catalytic proton transfer (Krebs et al., 1991).

The substitution of only slightly larger side chains for A65, such as threonine and serine, results in less dramatic structural changes in the environment of proton shuttle group H64. The difference electron density map of A65T CAII in Figure 5 reveals that the side chain of T65 is sufficiently short to allow both the in and out conformers of H64. These conformers are related by a 101° difference in side chain torsion angle $\chi_1$ and a 15° difference in side chain $\chi_2$ and refine with approximate occupancies of 40% and 60%, respectively. Importantly, the side chain of T65 is sufficiently short that it does not sterically require the displacement of water molecules 264, 292, and 369. The side chain hydroxyl group of T65 donates a hydrogen bond to the backbone carbonyl of F95 and accepts a hydrogen bond from the backbone amide NH of F66. Interestingly, the nonprotein zinc ligand in this structure is characterized by cigar-shaped electron density (data not shown) and appears to be an azide anion (present during protein purification). The binding of azide is comparable to that observed in its complex with the native enzyme (Nair & Christianson, 1993) and requires the displacement of the so-called "deep" water molecule found at the mouth of the hydrophobic pocket (Håkansson et al., 1992). Azide anion is held in place by zinc coordination, a hydrogen bond interaction with the backbone NH of T199, and a non-hydrogen-bonded van der Waals contact with the side chain OH group of T199.

The electron density map of A65S CAII (data not shown) reveals that the side chain hydroxyl of S65 occupies the same location as that of T65, and this conformation is identical in

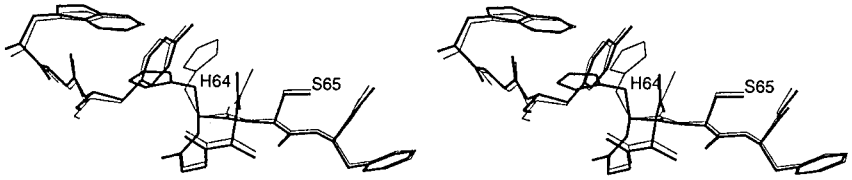


FIGURE 6: Least-squares superposition of monoclinic (thin bonds) and orthorhombic (thick bonds) A65S CAII structures. H64 adopts the in conformation in the monoclinic structure and the out conformation in the orthorhombic structure.

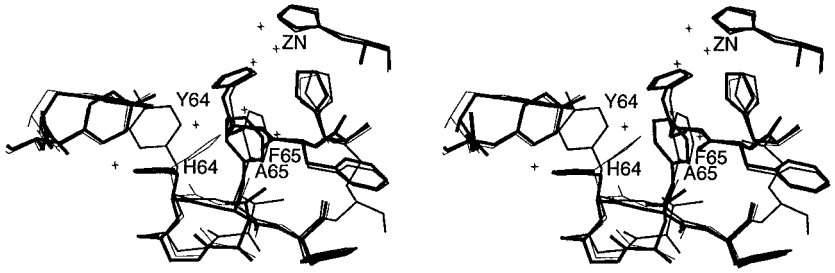


FIGURE 7: Least-squares superposition of A65F CAII (thick bonds), native CAII (thin bonds), and wild-type murine CAV (medium bonds). Residues 64 and 65 are indicated. Solvent molecules from the native structure are represented by unlabeled crosses.

both the monoclinic and orthorhombic crystal forms of A65S CAII. Like the side chain of T65, the hydroxyl group of S65 donates a hydrogen bond to the backbone carbonyl of F95 and accepts a hydrogen bond from the backbone amide NH of F66 in each structure. The side chain of S65 is not sufficiently large to require the displacement of water molecules 264, 292, and 369, nor does it perturb the in conformation of H64 in the monoclinic crystal form. However, H64 occupies the out conformation in the orthorhombic crystal structure of A65S CAII. The two H64 conformers in the monoclinic and orthorhombic crystal structures are related by an 81° difference in side chain torsion angle $\chi_1$ and a 23° difference in side chain torsion $\chi_2$. The rms deviation of Cα atoms between the monoclinic and the orthorhombic structures is 0.33 Å (Figure 6). A region of particular flexibility is the polypeptide backbone of flanking residue H36, which shifts as much as 1 Å. This conformational change appears to be due to a hydrogen bond observed between the backbone carbonyl of H36 and the Nζ of K170 in the symmetry-related molecule at $-x$, $y + {}^1/_2$, $-z + {}^1/_2$) in the orthorhombic structure.

In contrast to the orthorhombic crystal structures of H94C and H94D CAIIs (Ippolito et al., 1995), the orthorhombic crystal structure of A65S contains a fully occupied zinc ion in the enzyme active site. Therefore, the occupancy of the active site zinc ion is *not* the primary feature affecting the crystallization of CAII variants in the orthorhombic crystal form, as previously hypothesized (Alexander et al., 1993; Ippolito et al., 1995). However, similar features of mobility are found among the three orthorhombic crystal structures. Three polypeptide segments of orthorhombic A65S CAII have significantly higher *B*-factors than the corresponding segments in the monoclinic crystal form of each variant: V37−S50, F70−K80, and K225−L240. Although the electron density for these loops is well ordered and continuous, the increased *B*-factors may reflect interlattice interactions specific to the orthorhombic space group.

Finally, the electron density map of A65G CAII shows that the deletion of the A65 side chain does not affect the conformation of H64, which therefore remains in the in conformation (data not shown). Additionally, the A65G substitution does not sterically perturb the formation of a solvent bridge between H64 and zinc-bound solvent. The nonprotein zinc ligand in this structure appears to be azide anion, as observed in the structure of the A65T variant. In both A65G and A65T CAIIs, azide is held in place by zinc coordination, a hydrogen bond interaction with the backbone NH group of T199, and a non-hydrogen-bonded van der Waals contact with the hydroxyl group of T199.

Analysis of this series of six crystal structures reveals the following trend: amino acid substitutions for A65 (except glycine) protrude to some degree into the catalytic proton transfer pathway. Large, bulky side chains at position 65 (such as phenylalanine, leucine, or histidine) sterically hinder the formation of an optimal solvent bridge between zinc-bound water and H64 like that observed in the native enzyme (Figure 1; Håkansson et al., 1992). Although these substitutions sterically force catalytic proton shuttle H64 to the out conformation, the conformation of H64 is not the feature responsible for perturbing $k_{cat}$: prior work demonstrates that normal $k_{cat}$ values are measured for T200S CAII, in which H64 resides predominantly in the out conformation with no perturbation of active site solvent structure (Krebs et al., 1991). Instead, compromised $k_{cat}$ values in A65F, A65L, and A65H CAIIs arise solely from the perturbation of active site solvent structure between zinc-bound solvent and H64. The linear and angular deformation of hydrogen bonds in a solvent network can dramatically diminish proton transfer (Scheiner, 1981). Consistent with this conclusion is the dependence of log($k_{cat}$) on residue 65 side chain volume—the bigger the side chain, the greater the perturbation of catalytically optimal solvent structure and the greater the compromise of proton transfer (Jackman, et al., 1996).

It is interesting to view structure−activity relationships for A65 CAII variants in view of the entire family of CA isozymes, in which sequence alignment shows significant divergence at position 65 (Table 1). This leads to significant active site structural differences which potentially affect the trajectory of catalytic proton transfer. For example, comparison of the A65F CAII and wild-type CAV structures suggests that F65 alters the steric contour of the active site sufficiently enough to block, or at least hinder, effective solvent-mediated proton transfer between zinc-bound water and residue 64 (H64 in CAII, Y64 in CAV) (Boriack-Sjodin et al., 1995). A least-squares superposition of wild-type CAV, A65F CAII, and native CAII clearly shows that wild-

type F65 of CAV and F65 of the A65F CAII variant are structurally homologous (Figure 7): each F65 side chain must sterically displace water molecules adjacent to residue 64, and each F65 side chain sterically forces adjacent residue 64 to adopt an out conformation. Notably, H64 in A65F CAII and Y64 in wild-type CAV adopt different out conformations related by a 145° rotation about side chain torsion angle $\chi_1$.

Other isozymes contain polar amino acid side chains at position 65: CAIII and CAVI contain T65, while CAI, CAII other than human, CAIV, and CAVII have S65 (Table 1). Even though both threonine and serine chains are bulkier than alanine, solvent-mediated proton transfer between zinc-bound solvent and H64 in T65 and S65 CAIIs is not blocked. Therefore, it is structurally feasible for residue 64 to play a role in proton transfer in other CA isozymes as long as residue 65 is no larger than threonine (Table 1). This conclusion is consistent with linear free energy relationships for A65 CAII variants reported by Jackman et al (1996). These isozymes include those indicated above except for CAI, where H200 is apparently the primary proton shuttle group (Engstrand et al., 1995).

## CONCLUSIONS

(1) Amino acid substitutions at position 65 of CAII demonstrate that the size of the side chain is critical for allowing the assembly of a bridging solvent network between zinc-bound solvent and shuttle residue H64. If the side chain of residue 65 is larger than threonine, the contour of the active site is sufficiently changed to hinder the formation of an optimal solvent network. This presumably results in solvent-mediated proton transfer via compensatory pathways, as revealed in the kinetic measurements of Jackman et al. (1996).

(2) The side chains of F65 or L65 are well above the critical size necessary to hinder proton transfer to H64 in the corresponding variants of CAII. Interestingly, CAV is the only carbonic anhydrase isozyme containing large amino acid side chains at position 65: phenylalanine is found in murine CAV and leucine is found in human CAV. Consistent with conclusions from the three-dimensional structure of murine CAV (Boriack-Sjodin et al., 1995; Boriack-Sjodin, 1996) and the results reported in this and the preceding paper-(Jackman et al., 1996), F65 of murine CAV and L65 of human CAV must block efficient proton transfer to Y64 of this particular isozyme. This is verified in recent site-directed mutagenesis experiments by Heck et al. (1996).

(3) From solely a structural perspective, H64 in other carbonic anhydrase isozymes including CAIV, CAVI, and CAVII can potentially function as an efficient proton shuttle due to the smaller side chains, such as serine or threonine, which have evolved at position 65. This structural conclusion is consistent with the kinetic properties measured for the A65S and A65T CAII variants (Jackman et al., 1996). The conclusive identification of catalytic proton shuttles in other carbonic anhydrase isozymes is certain to be the subject of future research efforts.

## REFERENCES


Alexander, R. S., Nair, S. K., & Christianson, D. W. (1991) *Biochemistry 30,* 11064−11072.

Alexander, R. S., Kiefer, L. L., Fierke, C. A., & Christianson, D. W. (1993) *Biochemistry 32,* 1510−1518.

Bacon, D., & Anderson, W. P. (1988) *J. Mol. Graphics 6,* 219−220.

Bernstein, F. C., Koetzle, T. F., Williams, G. J. B., Meyer, E. F., Brice, M. D., Rodgers, J. R., Kennard, O., Shimanouchi, T., & Tasumi, M. (1977) *J. Mol. Biol. 112,* 535−542.

Boriack-Sjodin, P. A. (1996) Ph.D. Dissertation, University of Pennsylvania, Philadelphia.

Boriack-Sjodin, P. A., Heck, R. W., Laipis, P. J., Silverman, D. N., & Christianson, D. W. (1995) *Proc. Natl. Acad. Sci. U.S.A. 92,* 10949−10953.

Brünger, A. T., Kuriyan, J., & Karplus, M. (1987) *Science 235,* 458−460.

Christianson, D. W., & Fierke, C. A. (1996) *Acc. Chem. Res. 29,* 331−339.

Collaborative Computational Project 4 (1994) *Acta Crystallogr. D50,* 760−763.

Engstrand, C., Jonsson, B.-H., Lindskog, S. (1995) *Eur. J. Biochem. 229,* 696−702.

Fleming, R. E., Crouch, E. C., Ruzicka, C. A., & Sly, W. S. (1993) *Am. J. Physiol. 265,* L627−L635.

Håkansson, K., Carlsson, M., Svensson, L. A., & Liljas, A. (1992) *J. Mol. Biol. 227,* 1192−1204.

Heck, R. W., Tanhauser, S. M., Manda, R., Tu, C. K., Laipis, P. J., & Silverman, D. N. (1994) *J. Biol. Chem. 269,* 24742−24746.

Heck, R. W., Boriack-Sjodin, P. A., Qian, P. A., Tu, C. K., Christianson, D. W., Laipis, P., & Silverman, D. N. (1996) *Biochemistry* (in press).

Hewett-Emmett, D., Hopkins, P. J., Tashian, R. E., & Czelusniak, J. (1984) *Ann. N.Y. Acad. Sci. 429,* 338−358.

Ippolito, J. A., Nair, S. K., Alexander, R. S., Kiefer, L. L., Fierke, C. A., & Christianson, D. W. (1995) *Protein Eng. 8,* 975−980.

Jackman, J. E., Merz, K. M., Jr., & Fierke, C. A. (1996) *Biochemistry 35,* 16421−16428.

Jewell, D. A., Tu, C. K., Paranawithana, S. R., Tanhauser, S. M., LoGrasso, P. V., Laipis, P. J., & Silverman, D. N. (1991) *Biochemistry 30,* 1484−1490.

Khalifah, R. G. (1971) *J. Biol. Chem. 246,* 2561−2573.

Kraulis, P. J. (1991) *J. Appl. Crystallogr. 24,* 946−950.

Krebs, J. F., Fierke, C. A., Alexander, R. S., & Christianson, D. W. (1991) *Biochemistry 30,* 9153−9160.

Leslie, A. G. W. (1992) *CCP4 and ESF-EACMB Newsletter on Protein Crystallography,* Vol. 26.

Lindskog, S., & Liljas, A. (1993) *Curr. Opin. Struct. Biol. 3,* 915−920.

Lindskog, S., Engberg, P., Forsman, C., Ibrahim, S. A., Jonsson, B. H., Simonsson, I., & Tibell, L. (1984) *Ann. N.Y. Acad. Sci. 429,* 62−75.

Merritt, E. A., & Murphy, M. E. P. (1994) *Acta Crystallogr. D50,* 869−873.

Nair, S. K., & Christianson, D. W. (1991) *J. Am. Chem. Soc. 113,* 9455−9458.

Nair, S. K., & Christianson, D. W. (1993) *Eur. J. Biochem. 213,* 507−515.

Navaza, J. (1994) *Acta Crystallogr. A50,* 157−163.

Read, R. J. (1986) *Acta Crystallogr. A42,* 140−149.

Sack, J. S. (1988) *J. Mol. Graphics 6,* 224−225.

Scheiner, S. (1981) *J. Am. Chem. Soc. 103,* 315−320.

Silverman, D. N., & Lindskog, S. (1988) *Acc. Chem. Res. 21,* 30−36.

Steiner, H., Jonsson, B.-H., & Lindskog, S. (1975) *Eur. J. Biochem. 59,* 253−259.

Tu, C. K., Silverman, D. N., Forsman, C., Jonsson, B.-H., & Lindskog, S. (1989) *Biochemistry 28,* 7913−7918.


BI9617872